ROYAL SOCIETY OF CHEMISTRY

PAPER

Check for updates

Paraelectric behavior and lamellar ordering in zwitterion-polymer blends

Simranjeet Kaur, Vance E. Williams [ID] and Loren G. Kaake [ID] *

We report the synthesis and dielectric characterization of a zwitterionic compound based on two common ionic liquid moieties. This compound can be blended with poly(methyl methacrylate) (PMMA) to form thin films. At high zwitterion concentrations, elevated temperatures, and low frequencies, the films exhibit behavior typical of electrochemical double layers, despite the absence of free ions. Capacitance values are in the range of 10 μF cm^{-2} and do not depend on film thickness. At low temperatures, the films behave as linear dielectric materials with a dielectric constant of approximately 7. The transition between these two regimes is governed by a phase transition corresponding to the melting temperature of the zwitterion, as observed through differential scanning calorimetry (DSC) and polarized optical microscopy (POM). X-ray diffraction (XRD) analysis suggests that at low temperatures and high concentrations, zwitterions adopt a lamellar structure characterized by strong antiparallel interactions between lamellae, which inhibit a strong paraelectric response. As the temperature increases, the compounds no longer exhibit phase separation and can adopt a parallel configuration, resulting in high capacitance paraelectric behavior. Overall, the zwitterionic compound reported here shows promising behavior that can be well-understood from its thermophysical and morphological properties.

Introduction

Ionic liquids are versatile organic salts with melting points below 100 °C, with low volatility, non-flammability, high ionic conductivity, and thermal stability. These qualities make them ideal for applications in batteries, fuel cells, solar cells and energy storage devices, among others.[1–4] However, the high ionic conductivity of ionic liquids can hinder performance in devices like organic transistors due to ion migration into the semiconductor layer.[5–7] Zwitterions, which have covalently bound cationic and anionic groups, offer an alternative by minimizing the translational motion and making them promising for electrochemical applications.[7–12]

The large dipole moments associated with zwitterions allow them to exhibit high dielectric constants, with neat zwitterionic liquids showing the largest reported dielectric constant (>220).[11] However, strong electrostatic interactions in their crystalline solid state can reduce overall permittivity through the cancellation of their dipole moments.[13] While the enhanced molecular mobility and dielectric response are exhibited in the liquid state, zwitterions typically have high melting points, limiting their practical use.[12,14] Efforts to utilize the high dielectric constant have focused on lowering melting

points by incorporating additives,[15,16] performing structural modifications[8,14,17–20] or plasticizing zwitterionic polymers with water to weaken the intermolecular interactions.[21,22]

In our previous work,[13] we synthesized an *N*-imidazolium and sulfonyl(trifluoromethane sulfonyl)imide-based zwitterion (**EG2IM-TFSI**). The compound has a diethylene glycol side group, which successfully lowered the melting point below 100 °C, enabling the study of dielectric properties at moderate temperatures. Remarkably, blending the zwitterion with poly(methyl methacrylate) (PMMA) resulted in a dielectric film that exhibited a three order of magnitude increase in capacitance upon heating above the zwitterion's melting point. This high capacitance behavior was independent of film thickness and resulted from highly correlated dipole moments, producing capacitance values comparable to electrostatic double layers. This material also showed strong supercooling behavior which was possibly related to a pendant ethylene glycol side chain. Supercooling may offer advantages for some applications, but its inherent metastability, sensitive to thermal and mechanical disturbances, poses challenges for reliable and consistent performance.[23] Therefore, there is a need to develop new materials with minimal supercooling while maintaining low melting temperature.

The imidazolium cation and sulfonyl(trifluoromethane sulfonyl)imide anion are promising candidates for reducing the melting temperature. In addition, the side chain of the

Department of Chemistry, Simon Fraser University, 8888 University Drive, Burnaby, BC, V5A 1S6, Canada. E-mail: lkaake@sfu.ca

zwitterions also significantly affects the thermal properties. For example, moderately long alkyl chain groups (C6–C8) in zwitterions have been shown to lower the melting point.[7] For linear ionic liquids, the melting point typically decreases with increasing alkyl chain length, reaching a minimum around eight carbon atoms, before rising again due to stronger van der Waals interactions between chains.[24] However, while low melting temperatures are desirable, ionic liquids with intermediate alkyl chain lengths also exhibit a high tendency for supercooling.[25] In polypeptoids, branched alkyl chains tend to lower the melting point more effectively than linear chains.[26,27] In contrast, branched ionic liquids often show higher melting points, T_g, and viscosities compared to their linear counterparts, due to more efficient local packing.[28–30] Meanwhile, branching in small organic compounds is generally associated with enhanced supercooling behavior[31,32] however, the effect of branching on supercooling in ionic liquids has not been directly reported.

Building on these observations, we note that moderately long linear alkyl chains can decrease the melting point in zwitterions but also promote supercooling. Therefore, we are particularly interested in the branched 2-ethyl-1-hexyl (**EH**) group, which is known to strongly influence molecular packing in polymer matrices and dramatically affect material properties.[26,33,34] Moreover, 2-ethylhexyl group are expected to be more hydrophobic than the previously used diethylene glycol group, offering better control over handling the material under ambient conditions without interference from absorbed water. In this work, we synthesized and characterized a zwitterionic compound with a branched 2-ethyl-1-hexyl alkyl chain which showed minimum supercooling. The thermophysical behavior of this compound was significantly more reversible than previous reports. In addition, when blended with PMMA, films showed a high, thickness independent capacitance. This behavior was observed at high concentrations and elevated temperatures in a manner similar to previous reports. These insights demonstrate the role of side chains in the structure–property relationship governing zwitterionic dielectric materials.

Materials and methods

PMMA (M_w 120 000), acetone, acetonitrile and isopropanol (HPLC grade solvents) were purchased from Sigma Aldrich. Hydrochloric acid was purchased from VWR chemicals. Titanium (Ti) metal sheet was purchased from McMaster-Carr, 0.05 mm diameter (99.995%) gold wire was purchased from Alfa Aesar, gold deposition material (99.999%) was purchased from Kurt J. Lesker. Deionized water was obtained from Barnstead Easypure II UV/VF water purification system. All commercially available solvents and chemicals were used as received. **EHIM-TFSI** was synthesized based on previously reported procedures.[13,35,36]

Square (1.5 cm × 1.5 cm) Ti metal substrates were cleaned, and films were prepared as reported in our previous work. PMMA was dissolved in acetonitrile (100 mg mL^{-1}) by stirring at 60 °C for 2 hours. The zwitterion was dissolved in PMMA

solution at the desired concentration (0.02–0.19 mol ratios), by stirring at 60 °C for 2 hours. The resulting zwitterion solution was then spin-coated on a titanium substrate at 1500 rpm for 60 s at room temperature. The samples were annealed at 120 °C for 1 hour. A gold circular top contact with a 3 mm diameter and 60 nm thickness was deposited through a shadow mask onto the film *via* physical vapor deposition using a system situated in a glovebox. The resulting devices were of asymmetric metal-insulator-metal (MIM) configuration.

The dielectric properties of spin-coated films on Ti substrates were measured using Solartron 1260A impedance analyzer attached to 1296 dielectric interface as a function of frequency (between 1 Hz and 1 MHz) and temperature (between 20 °C and 130 °C) at 1 V. Gold wires were attached to the top gold electrode and bottom Ti electrode using silver paste dissolved in amyl acetate. The high-temperature measurements were performed using Delta 9015 furnace, where samples were heated at a rate of 20 °C min^{-1} and held for 5 minutes. All measurements were conducted in air. To perform thickness dependent measurement for 0.15 mol ratio of **EHIM-TFSI**, the films were cast from different concentrations of PMMA (100 mg, 150 mg, 200 mg and 250 mg) in 100 mL acetonitrile using abovementioned spinning conditions, which resulted in a variation of sample thicknesses. The polarization–voltage hysteresis loops were measured on the same samples using a ferroelectric analyser (Radiant RT66A Standard Ferroelectric Testing System) at 10 Hz at variable temperatures which were achieved using the aforementioned Delta 9015 furnace.

Phase transitions were investigated using a Q200 DSC instrument (TA Instruments) equipped with a Refrigerated Cooling System 90. The films were drop-cast onto 1.5 × 1.5 cm clean glass substrates from solutions identical in composition to those used for impedance measurements and dried at room temperature for 3 days before annealing at 120 °C for 1 hour. Approximately 2–3 mg of film was obtained and placed into a Tzero aluminum pan and sealed. Heating and cooling measurements were performed on these films and pure zwitterion compound at a rate of 10 °C min^{-1}.

The samples for polarized optical microscopy (POM) were spin cast from a 100 mg mL^{-1} PMMA solution on 1.5 × 1.5 cm cleaned glass substrates, followed by annealing using the previously described recipe. The texture and phase behavior of these films were analyzed using an Olympus BX50 microscope equipped with a Linkam LTS350 heating stage, a TMS94 temperature controller and a first order, full wave, gypsum plate of 530 nm (Olympus U-TP530). The samples were heated at a rate of 5 °C min^{-1} and maintained for 3 minutes at target temperature before images were collected.

The samples for X-ray diffraction (XRD) and Fourier transform infrared spectroscopy (FTIR) measurements were prepared in a similar way as for POM measurements, but by casting films from a 250 mg mL^{-1} PMMA solution onto clean glass substrates (1.5 cm × 1.5 cm). The crystallinity in films was determined using XRD on a high-resolution Bruker D8 Advance diffractometer with a copper Kα1 X-ray tube. The thin films were scanned from 2θ = 3° to 30° at 5° min^{-1}. Additionally, 2d

Medium Angle X-ray Scattering (MAXS) experiments were performed on films taken from glass substrates and collected using SAXSLAB Ganesha 300XL small angle X-ray scattering system. FTIR measurements were also performed on films taken from glass substrates and measured using a PerkinElmer infrared spectrometer.

Film thicknesses were measured using a Bruker Dektak XT profilometer equipped with Vision 64 software. The stylus had a 2.0 μm tip diameter, scanned at 30 μm s^{-1} with a force of 3 mg. Thickness was measured as the step height between areas with and without film on glass substrates. Thickness values are provided in Table S1.

Results and discussion

To explore the role of side chains in the properties of zwitterion containing thin films, we synthesized a compound containing a branched alkyl side chain. Fig. 1 shows the route for synthesizing the compound, hereafter referred to as **EHIM-TFSI**. The compound was synthesized using *N*-2-ethyl-1-hexyl imidazole and potassium chlorotrifluoromethylsulfonyl chloride using procedures adopted from literature;[13,35,36] the complete synthesis and characterization provided in Fig. S1–S4.

When compared with a compound with ethylene glycol side chains (**EG2IM-TFSI**), the melting point of **EHIM-TFSI** increased to 120 °C (Fig. 2). Importantly, this slight increase in melting point is still significantly lower than the melting points typically observed in traditional zwitterions which can exceed 250 °C. The branched alkyl group provides steric hindrance, allowing for some degree of rotation similar to the diethylene glycol group, which inhibits intermolecular interactions, reducing packing efficiency.

Significantly, **EHIM-TFSI** exhibits minimal supercooling which significantly improved the thermal reversibility of the system compared to previous system as confirmed by comparing the DSC result of two compounds (Fig. 2). The enhanced thermal reversibility allows for more stable performance across thermal cycles, improving the material's durability and reproducibility upon repeated cycles. We hypothesize that the differences in the thermal behavior between the two compounds result from the lower affinity of the alkyl chain to the ionic groups. This reduces the interaction between the side chains and neighboring molecules, reducing the cooperativity of the crystallization process.[12,19]

Dielectric properties are a key characteristic of zwitterion-containing thin films. To examine if **EHIM-TFSI** exhibits these properties, thin films were prepared by blending **EHIM-TFSI** with PMMA, and spin-coating the resulting solutions onto Ti substrates. Ti was chosen as the substrate due to its relatively
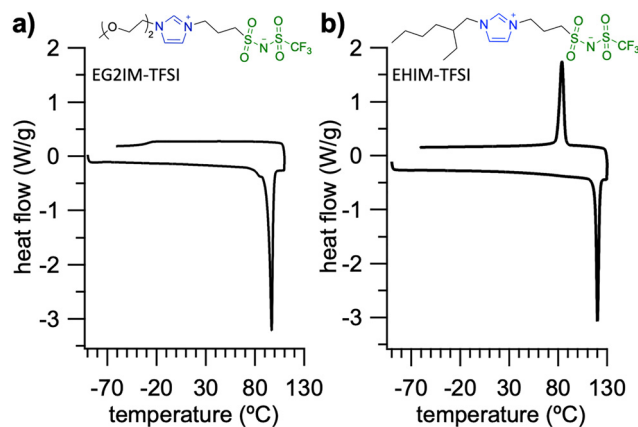

Fig. 2 DSC plots of (a) **EG2IM-TFSI** and (b) **EHIM-TFSI**.

low cost, as well as its chemical stability and corrosion resistance. The selection of a suitable polymer matrix for zwitterions is limited by compatibility with both the zwitterion and the solvent used to form solutions. Low dielectric constant PMMA was selected due to its high mechanical strength, transparency, chemical stability, processability, and hydrophobicity.[37] Solutions of zwitterion and PMMA were created in acetonitrile with 100 mg mL^{-1} of PMMA at the following mol ratios of zwitterion: 0, 0.02, 0.05, 0.11, 0.15 and 0.19. Films were spin coated at 1500 rpm, resulting in films that were in range 1–2.5 μm (Table S1). The increase in film thickness was the result of an increase in solution viscosity with a greater **EHIM-TFSI** mol ratio. The thickness dependent dielectric properties will be discussed later.

To evaluate **EHIM-TFSI**'s dielectric performance, a gold electrode was vapor deposited onto the films, and frequency-dependent capacitance was measured across several temperatures at 1 V. The capacitance (F cm^{-2}) was calculated from the imaginary impedance Z'' using the eqn (1), where f is the frequency and A is the area of the top electrode.

$$C = \frac{-1}{2\pi f Z'' A} \tag{1}$$

Fig. 3(a)–(f) show the variation of capacitance with frequency at different temperatures and concentrations of **EHIM-TFSI**. Fig. 3(a) shows the response of a pure PMMA thin film. The capacitance is approximately 5 nF cm^{-2} and independent of frequency with a slight increase observed at higher temperatures due to segmental motion of the polymer aligning the polar ester groups with the electric field (Fig. S5(a)).[38] When **EHIM-TFSI** is added at low concentrations (Fig. 3(b)), the film exhibits a small temperature-dependent increase in capacitance, similar to pure PMMA. This is consistent with previous findings,[13] that the uncorrelated dipole moments of **EHIM-TFSI** have a small effect on capacitance, which becomes more pronounced as temperature rises. Films with higher concentrations of **EHIM-TFSI** (Fig. 3(c)–(f)) show a much stronger temperature dependence, with low-frequency capacitance increasing by a factor of 1000 from 20 °C to 130 °C at and above 0.1 mol ratio. This behavior is also consistent with our previous system,[13] where capacitance above the melting point
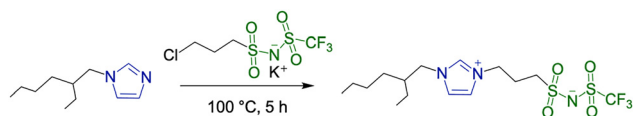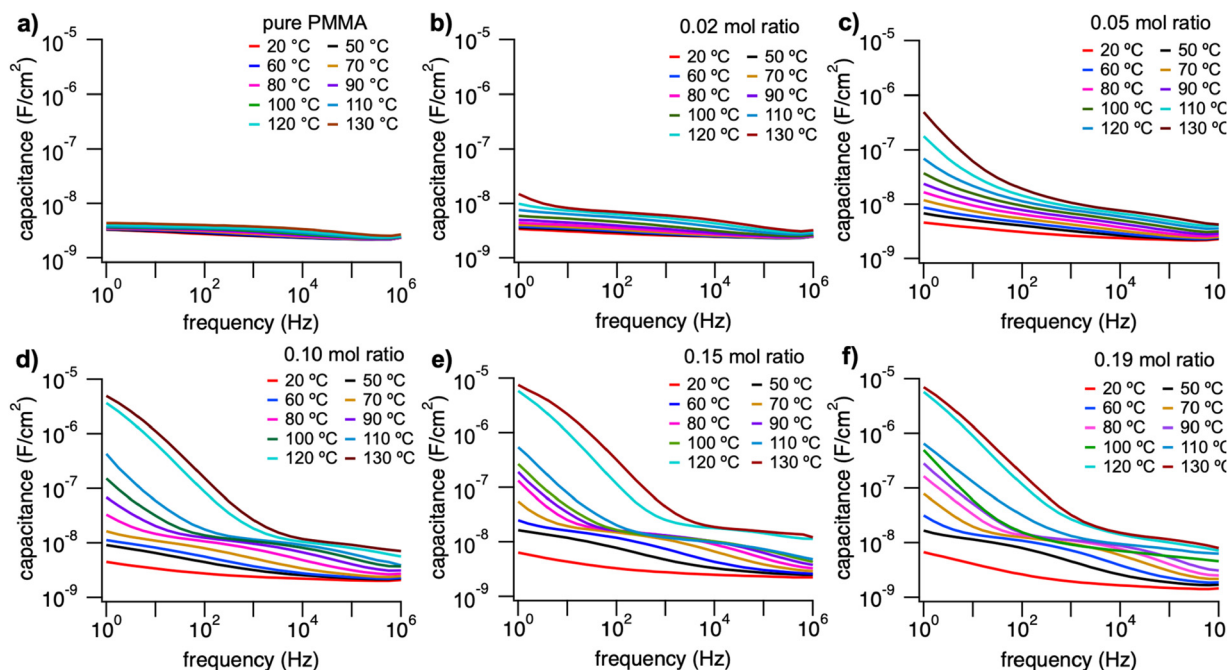

Fig. 1 Synthetic pathway of **EHIM-TFSI**.

Fig. 3 Capacitance *vs.* frequency at different temperatures at 1 V with films of different mol ratios of **EHIM-TFSI** in PMMA. (a) pure PMMA, (b) 0.02 mol ratio, (c) 0.06 mol ratio, (d) 0.11 mol ratio, (e) 0.15 mol ratio and (f) 0.19 mol ratio.

reaches values similar to ion gels formed by imidazolium bis(trifluoromethylsulfonyl)imide ionic liquids, which display a capacitance of 12.2 ± 0.9 μF cm^{-2} at 1 Hz.[39]

The films demonstrate excellent thermal reversibility, with minimal change in capacitance during subsequent heating and cooling cycles, as shown in Fig. S5. This behavior underscores the improved stability of compounds containing alkyl side chains, making them more suitable for practical applications that require consistent capacitance over multiple thermal cycles.

The impedance data for PMMA-**EHIM-TFSI** films was also analyzed using the Havriliak–Negami model (Fig. S6 and S7), which accurately describes the frequency-dependent behavior. The dielectric relaxation behavior is characterized by two primary components, a lower capacitance process occurring at high frequencies and a high capacitance process at lower

frequencies. The first relaxation process, characterized by lower capacitance (in nF cm^{-2}) in Fig. 3(d)–(f), shows a faster orientation response in films, which can be attributed to the polar side chains in PMMA, occurring in less than 1 μs at 120 °C. The second relaxation, with higher capacitance (in μF cm^{-2}) and a time constant of approximately 0.01 s above 120 °C for films with higher concentrations (≥ 0.1 mol ratio) is attributed to orientational polarization of the zwitterionic compounds, leading to the formation of an electrical double layer.

The complex impedance measurements of $\tan(\delta)$ (Fig. S8(b)–(f)) show a dielectric loss peak due to zwitterions in addition to β relaxation peak of PMMA (Fig. S8(a)). This peak decreases in intensity and shifts to higher frequencies as the temperature rises, indicating that the alignment of the highly polar zwitterionic molecules with the electric field becomes easier at higher
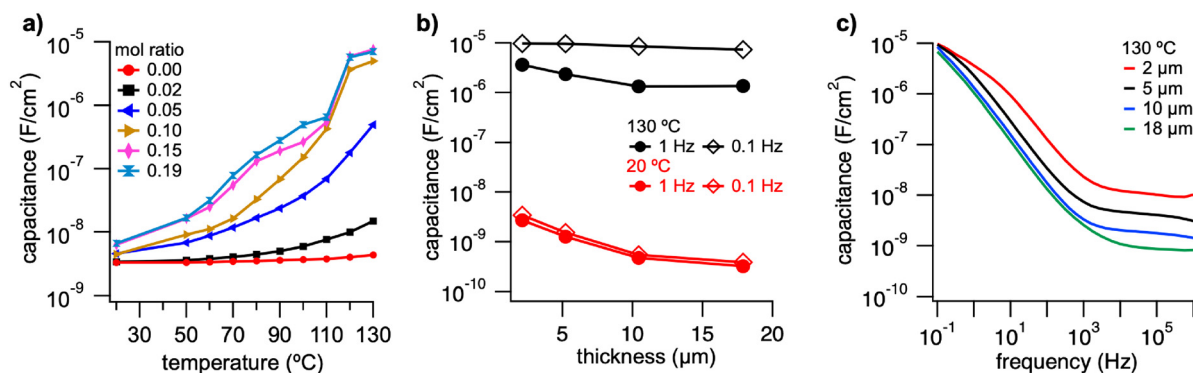

Fig. 4 (a) Capacitance *vs.* temperature for different concentrations at 1 Hz. (b) Capacitance vs thickness measurements of 0.15 mol ratio **EHIM-TFSI** blended film at different temperatures and frequencies. (c) Capacitance vs frequency measurements of 0.15 mol ratio **EHIM-TFSI** blended film at different thicknesses at 130 °C.

Journal of Materials Chemistry C

Paper

temperatures.[38] Moreover, polarization measurements (Fig. S9) on films with lower zwitterion concentrations exhibit paraelectric behavior, while high-concentration films show increased polarization and hysteresis loops, which we speculate may arise from contributions of both ferroelectric-like behavior and electrical conductivity.[40] However, it remains unclear whether these materials exhibit true ferroelectricity due to the complex interplay of zwitterion reorientation and polymer chain motion.

The effect of temperature on the capacitance at 1 Hz for several different concentrations of **EHIM-TFSI** is summarized in Fig. 4(a) and Fig. S10. At low concentrations, the capacitance is relatively small but increases with temperature. As the concentration increases, the capacitance response becomes more pronounced and increases gradually with increasing temperature. For higher concentrations (≥ 0.1 mol ratio), the capacitance increase is also gradual between 20 °C and 110 °C, but is followed by a more abrupt increase between 110 °C and 120 °C, which is near the melting point of zwitterion. The highest values obtained values of capacitance are consistent with the formation of an electrostatic double layer.[41–43]

To further investigate the electrostatic double layer phenomenon, Fig. 4(b) shows the thickness dependent capacitance measurements of 0.15 mol ratio **EHIM-TFSI** blended films at different temperatures and frequencies. At 20 °C, the film exhibits a capacitance that scales with the inverse thickness irrespective of frequency, as one would expect of a linear dielectric material. However, at higher temperatures (130 °C), the capacitance at 1 Hz is large and only decreases slightly with increasing film thickness. When the films are analyzed at an even lower frequency of 0.1 Hz, the capacitance becomes nearly constant, irrespective of the film thickness. This thickness-independent character of film at 0.1 Hz supports the hypothesis that the capacitance of zwitterion films is determined by their properties at the electrode interfaces alone. The frequency and temperature dependent capacitance and tan delta measurements of PMMA and 0.15 mol ratio **EHIM-TFSI** blended film of different thicknesses are provided in Fig. S11 (a)–(f) and S12 (a)–(f).

The existence of two clear frequency regimes in the capacitance is further demonstrated in Fig. 4(c) which displays the frequency dependence capacitance for 0.15 mol ratio **EHIM TFSI** films at 130 °C for several film thicknesses. High and thickness independent capacitance appears at low frequencies while low, thickness dependent capacitance is observed at high frequencies. Linear dielectric materials have a capacitance that depends inversely on the film thickness and is well-characterized by a bulk dielectric constant. As such, we hypothesize that the high frequency region of the impedance spectrum is characterized by approximately linear dielectric behavior with a relative dielectric constant of 7. In the limit of low frequency, thin film capacitance is independent of thickness, meaning that its properties cannot be described by a bulk dielectric constant. This is consistent with the hypothesis that the capacitance of zwitterion films is determined by their properties at the electrode interfaces alone.

To understand the temperature dependent behavior of the **EHIM-TFSI** films, DSC measurements were performed on blended samples prepared *via* drop-casting. At lower **EHIM-TFSI** loadings
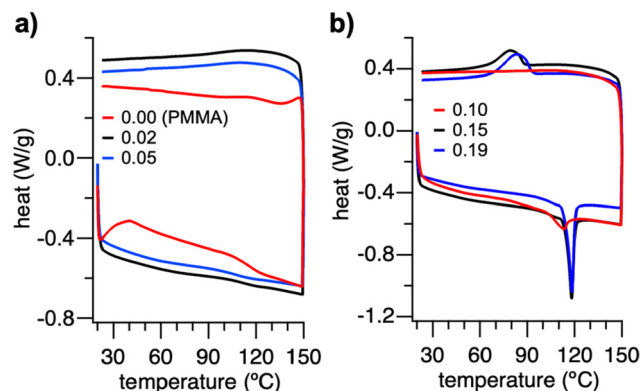

Fig. 5 DSC results at (a) low concentrations and pure PMMA film and (b) higher concentrations of **EHIM-TFSI** in PMMA.

(Fig. 5(a)), no endothermic peak was observed except for the T_g at 116 °C, similar to pure PMMA. We interpret this as an indication that the zwitterion molecules are well-dissolved in the polymer matrix. At the highest loadings (>0.1 mol ratio), a strong endothermic peak appears at approximately 120 °C in the DSC data shown in Fig. 5(b). The temperature of this peak coincides with the melting of the pure compound (Fig. 1(a)). This peak suggests the presence of crystalline regions of the zwitterion molecules in the blend at concentrations above 0.10, which correlates well with the concentration dependence of the high-capacitance behavior. During the cooling cycle shown in Fig. 5(b), an endothermic peak is observed at 80 °C, which we interpret as the recrystallization of **EHIM-TFSI** and a manifestation of the overall improved thermal cyclability of the compound. At 0.1 mol ratio, the material appears to behave in an intermediate manner between the high concentration and low concentration regimes.

In more detail, the T_g of PMMA shifts and broadens upon the addition of zwitterions to approximately 111 °C for 0.02 mol ratio and 107 °C for 0.06 mol ratio. We attribute this small shift to an increase in mobility of the polymer chains. At higher **EHIM-TFSI** concentrations (>0.1 mol ratio), T_g is difficult to observe, either because it overlaps with the melting peak of **EHIM-TFSI** or is significantly broadened. FTIR analysis (Fig. S13 and Table S2) shows that with increasing zwitterion content, the CO stretching peak of PMMA shifts to 4 cm^{-1} higher wavenumbers at 0.19 mol ratio, indicating some interaction between PMMA and zwitterion.

In order to further investigate the role of phase separation in **EHIM-TFSI**/PMMA blends, polarized optical microscope (POM) images of films were collected at 20 °C and 130 °C. Phase contrast was improved with a 530 nm retardation plate. The results are shown in Fig. 6. At concentrations ≤ 0.1 mol ratio (Fig. 6(b)–(d)), no phase separation is observed as indicated by a featureless magenta image indistinguishable from that of pure PMMA (Fig. 6(a)). This indicates that **EHIM-TFSI** is well-mixed within the PMMA film, in agreement with the DSC data.

On increasing temperature (Fig. 6(g)–(j)), images of these films do not change in any obvious way. This behavior is in contrast with images collected at higher concentrations (>0.1 mol ratio) as shown in Fig. 6(e) and (f). They display
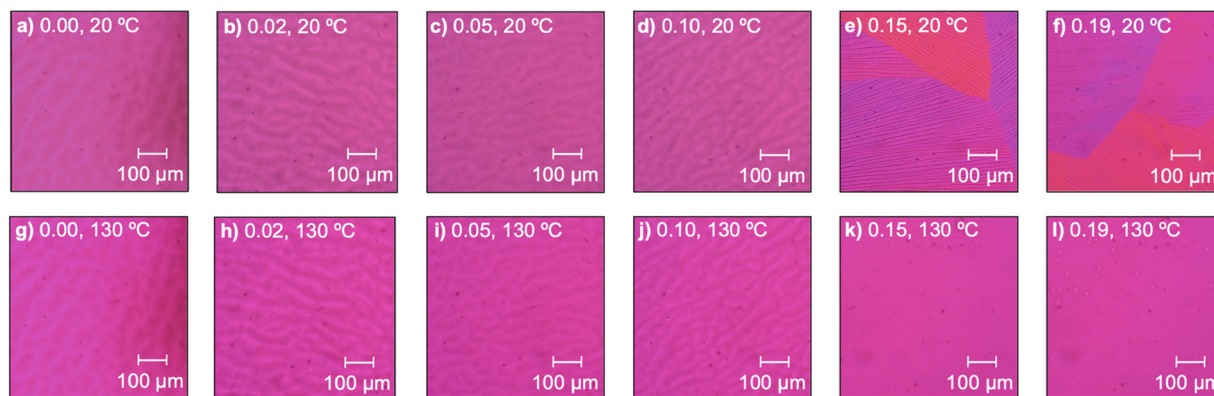
Fig. 6 Concentration dependent POM images. Images of (a) pure PMMA, (b) 0.02, (c) 0.05, (d) 0.10, (e) 0.15, and (f) 0.19 mol ratio of **EHIM-TFSI** in PMMA at 20 °C. Images of (g) pure PMMA, (h) 0.02, (i) 0.06, (j) 0.10, (k) 0.15, and (l) 0.19 mol ratio of **EHIM-TFSI** in PMMA at 125 °C. All images viewed through cross-polarizers with a 530 nm retardation plate.

bright purple/orange crystalline regions at 20 °C, corresponding to birefringent **EHIM-TFSI** enriched domains. At temperatures where EHIM-TSFI is observed to melt *via* DSC, these purple/orange domains become non-birefringent (as shown in Fig. 6(k) and (l)). These results correspond well with the observed phase behavior in the DSC experiments of Fig. 5 as well as the onset of high capacitance behavior observed in Fig. 3 and 4. Further analysis of the POM images can be found in the appendix (Fig. S14).

The presence of crystalline regions of **EHIM-TFSI** within spin coated thin films at room temperature was further investigated through XRD measurements. Fig. 7(a) shows the diffraction patterns for pure PMMA films and films with differing concentrations of **EHIM-TFSI**. At the lowest concentrations (below 0.1 mol ratio), the films are almost completely amorphous, in agreement with both the DSC and the POM images. These observations suggest that **EHIM-TFSI** is dispersed in the polymer matrix. At higher concentrations, a series of well-defined diffraction peaks emerge (2θ = 4.46, 8.93, 13.42 and 17.96), that we assign as the (001), (002), (003) and (004) peaks of a lamellar phase. This peak is also observed for the intermediate concentration of 0.1 mol ratio. The peak (as seen in the inset of Fig. 7(b)) is of low intensity, again pointing to this

concentration as intermediate to the two main categories of material behavior.

The observed patterns (as in Fig. 7(a)) remain almost unchanged for films at varying thicknesses and cooling rate of the annealed film. This suggests that zwitterions tend to crystallize in a reproducible manner, regardless of the presence of PMMA-rich domains. To analyze these effects, additional experiments are detailed in appendix (Fig. S17–S19). To investigate the azimuthal ordering of **EHIM-TFSI**, medium angle X-ray scattering (MAXS) measurements were performed. The results, shown in Fig. 7(c) are characterized by circular rings at q = 0.32 A^{-1} (2θ = 4.45 nm) in the *XY* scatter plot, indicating a lack of azimuthal ordering.

With respect to the XRD data shown in Fig. 7(a) and (b), the peak at 2θ = 4.46 has a *d*-spacing equivalent to 1.98 nm, which is approximately equal to the length of the fully extended **EHIM-TFSI** molecule (Fig. S15). We hypothesize that the first-order lamellar peak at 2θ = 4.46° arises from long-range lamellar ordering. Although branched side chains would typically be expected to disrupt ordered packing, both our result and literature[44] show that in certain systems they can instead promote long-range lamellar organization. This is shown schematically in Fig. 8a using a black arrow and a representative
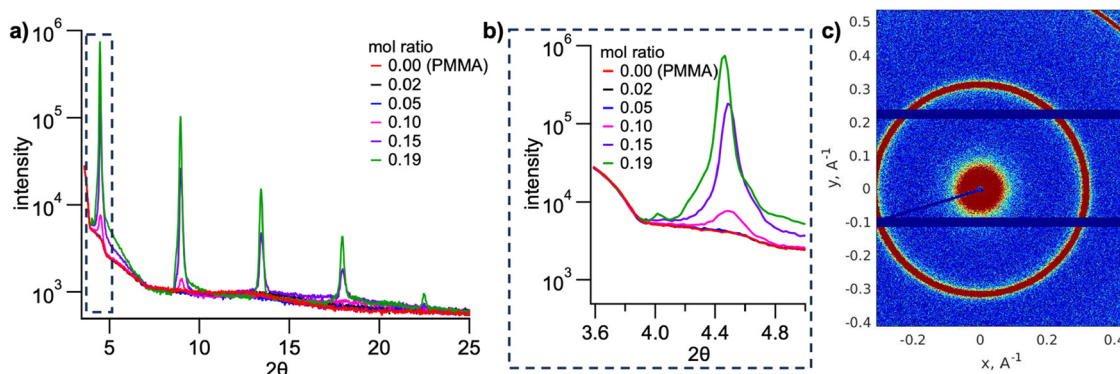

Fig. 7 (a) XRD plots of **EHIM-TFSI** blended films at different concentrations, and (b) zoomed-in XRD plot showing first order diffraction peaks from all concentrations. (c) *XY* scatter MAXS plot of **EHIM-TFSI**/PMMA film at 0.15 mol ratio.
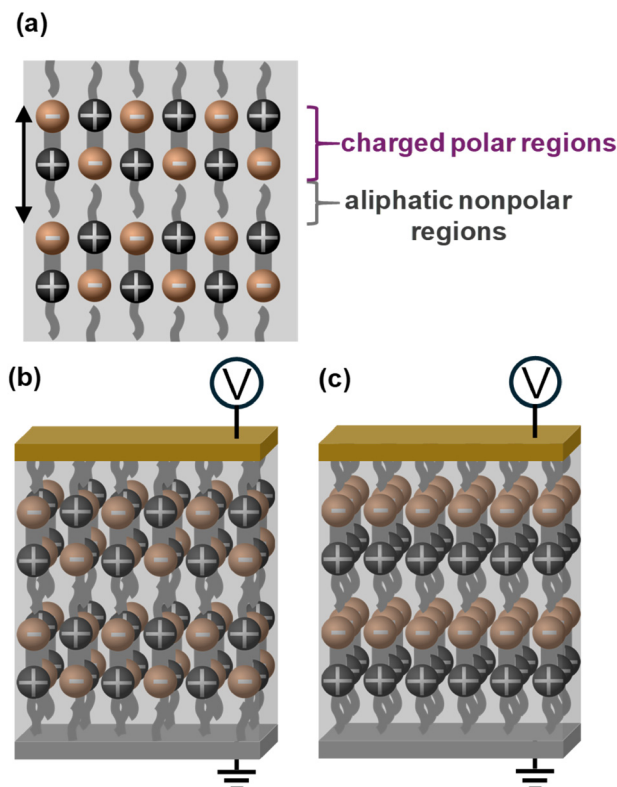
Fig. 8 (a) Proposed molecular arrangement of zwitterions in PMMA at room temperature, with black arrow indicating the first-order lamellar peak ($2\theta = 4.46°$) and separation of polar and nonpolar regions. Under electric field, the configuration of zwitterion molecules (b) below and (c) above the melting temperature of zwitterion **EHIM-TFSI**.

cartoon of the proposed structure. In this structure, **EHIM-TFSI** molecules are packed end-to-end between the lamellae in the film, with each adjacent molecule aligned in an antiparallel fashion at room temperature. The parameter $d = 1.98$ nm describes the interlamellar spacing, as shown in Fig. 8(a). This configuration results in the segregation of polar and non-polar regions within the zwitterionic PMMA film, which is favored by aggregation of ethyl hexyl chains.[12] Other possible configurations, described in Fig. S20, appear less probable.

We hypothesize that the dominant polarization mechanism at and above the melting temperature in **EHIM-TFSI**:PMMA blends is the formation of an electric double layer, which can be considered a type of interfacial polarization. This is an effect of dipolar polarization from the reorientation of zwitterions under the applied alternating field. Under these conditions, the net electric field within the film approaches zero due to cancellation by positive and negatively charged functional groups, resulting in charge accumulation primarily at the interfaces. XRD analysis provides additional insight, revealing that these zwitterions are microstructurally ordered in lamellar arrangements within the PMMA matrix. This lamellar ordering, as illustrated in Fig. 8(c), facilitates the formation of electric double layers that lead to interfacial charges.

In greater detail, the properties of our films can be understood by their local morphology. At room temperature, dipoles align antiparallel to each other, effectively canceling out the net dipole moment (Fig. 8(b)). This arrangement is due to strong intermolecular electrostatic interactions even under an applied electric field (1 V in this case). This antiparallel ordering likely contributes to the low capacitance observed at room temperature. However, when the film is heated to above its melting point and subjected to an electric field, the zwitterions can reorient in response to the field, maximizing their net dipole moment. This molecular reconfiguration leads to the formation of an electrical double layer at the electrode interfaces, leading to higher capacitance, as depicted in Fig. 8(c).

The temperature-dependent XRD measurements (Fig. S16(b) and (c)), conducted without an electric field, show that the peak intensity at $2\theta = 4.46$ gradually decreases between 80 °C and 110 °C and disappears entirely at 120 °C, indicating a loss of molecular order upon melting. This conclusion is supported by observations of high, thickness independent, capacitance as indicative of the presence of an electrical double layer.

To understand in how molecules are arranged in PMMA matrix, it is also worthwhile to consider the composition in terms of volume fraction, rather than mole or weight fraction. The molar volume of PMMA monomer units is usually considered 84.9 cm^3 mol^{-1}.[45] An **EHIM-TFSI** molecule can occupy 265.5 cm^3 mol^{-1} in extended form (as calculated from DFT). The films with zwitterion concentration of mol fractions 0.02, 0.05, 0.10, 0.15 and 0.19 correspond to volume fraction 0.07, 0.15, 0.27, 0.35 and 0.42, respectively. This means, below 27%, the dipoles can be imagined to be mostly isolated. To achieve high capacitance optimal alignment must occur, requiring that the dipoles have a correlated orientation in one direction. This is facilitated by the film bulk containing at least 27% zwitterion. At this volume fraction, the solubility limit has been reached, and percolating clusters of zwitterion crystals are able to reach across the film thickness providing the observed high capacitance behavior.

Conclusion

We have synthesized **EHIM-TFSI**, a heretofore unreported zwitterionic compound, and blended it with PMMA to form thin films. These films were characterized according to their dielectric properties. The observed capacitance at high temperatures, high **EHIM-TFSI** concentrations, and low frequencies is equivalent to that of an electrostatic double layer. This is further demonstrated by thickness independent values of the capacitance under these conditions. At higher frequencies, capacitance is better characterized in terms of linear dielectric behavior, exhibiting a dielectric constant of approximately 7. At low concentrations, **EHIM-TFSI** zwitterions are well dissolved in PMMA, exhibiting modest dielectric performance consistent with a linear dielectric. The temperature crossover between the two regimes of operation corresponds to the melting temperature of **EHIM-TFSI**. XRD analysis indicates that the strong antiparallel interactions between zwitterion molecules in zwitterion-rich lamellar domains are responsible for the low capacitance at lower temperatures and high zwitterion

concentrations. Despite the common tendency of zwitterions and branched alkyl chains in organic systems to undergo supercooling, our synthesized **EHIM-TFSI** zwitterion demonstrates a significantly low melting point and minimal supercooling. This enhanced thermal reversibility contributes to stable performance across multiple thermal cycles, increasing the material's durability and making it highly suitable for applications requiring reliable and reproducible thermal response.

Conflicts of interest

There are no conflicts to declare.

Data availability

Data can be made available upon request.

The SI contains information on synthetic procedures and chemical characterization. Characterization of the film structure, performance, and analysis of frequency dependent capacitance measurements using the Havriliak–Negami equation is also contained in the SI. See DOI: **https://doi.org/10.1039/d5tc02312b**

References

1 M. Watanabe, M. L. Thomas, S. Zhang, K. Ueno, T. Yasuda and K. Dokko, Application of Ionic Liquids to Energy Storage and Conversion Materials and Devices, *Chem. Rev.*, 2017, **117**, 7190–7239.

2 G. Kaur, H. Kumar and M. Singla, Diverse applications of ionic liquids: A comprehensive review, *J. Mol. Liq.*, 2022, **351**, 118556.

3 T. Zhou, C. Gui, L. Sun, Y. Hu, H. Lyu, Z. Wang, Z. Song and G. Yu, Energy Applications of Ionic Liquids: Recent Developments and Future Prospects, *Chem. Rev.*, 2023, **123**, 12170–12253.

4 H. A. Elwan, R. Thimmappa, M. Mamlouk and K. Scott, Applications of poly ionic liquids in proton exchange membrane fuel cells: A review, *J. Power Sources*, 2021, **510**, 230371.

5 J. Lee, L. G. Kaake, J. H. Cho, X.-Y. Zhu, T. P. Lodge and C. D. Frisbie, Ion Gel-Gated Polymer Thin-Film Transistors: Operating Mechanism and Characterization of Gate Dielectric Capacitance, Switching Speed, and Stability, *J. Phys. Chem. C*, 2009, **113**, 8972–8981.

6 J. D. Yuen, A. S. Dhoot, E. B. Namdas, N. E. Coates, M. Heeney, I. McCulloch, D. Moses and A. J. Heeger, Electrochemical Doping in Electrolyte-Gated Polymer Transistors, *J. Am. Chem. Soc.*, 2007, **129**, 14367–14371.

7 M. Yoshizawa-Fujita and H. Ohno, Applications of Zwitterions and Zwitterionic Polymers for Li-Ion Batteries, *Chem. Rec.*, 2023, **23**, e202200287.

8 M. Yoshizawa, A. Narita and H. Ohno, Design of Ionic Liquids for Electrochemical Applications, *Aust. J. Chem.*, 2004, **57**, 139.

9 M. K. Alsaedi, B. D. Like, K. W. Wieck and M. J. Panzer, Zwitterionic Materials for Enhanced Battery Electrolytes, *ChemPlusChem*, 2024, **89**, e202300731.

10 J. Liu, Y. Xu, F. Xu, J. Li, Y. Chen, J. Qiao, Y. Han, Y. Ren and B. Lin, Zwitterionic poly(ionic liquids)-based polymer electrolytes for Lithium-ion batteries applications, *Ionics*, 2023, **29**, 2249–2259.

11 W. Mei, A. J. Rothenberger, J. E. Bostwick, J. M. Rinehart, R. J. Hickey and R. H. Colby, Zwitterions Raise the Dielectric Constant of Soft Materials, *Phys. Rev. Lett.*, 2021, **127**, 228001.

12 W. Mei, A. Han, R. J. Hickey and R. H. Colby, Effect of chemical substituents attached to the zwitterion cation on dielectric constant, *J. Chem. Phys.*, 2021, **155**, 244505.

13 S. Kaur, R. M. D'Souza, T. L. Kelly, V. E. Williams and L. G. Kaake, Electrostatic Correlations Lead to High Capacitance in Zwitterion-Containing Thin Films, *ACS Appl. Mater. Interfaces*, 2024, **16**, 38290–38299.

14 H. Ohno, M. Yoshizawa-Fujita and Y. Kohno, Design and properties of functional zwitterions derived from ionic liquids, *Phys. Chem. Chem. Phys.*, 2018, **20**, 10978–10991.

15 H. Park, H. S. Kim and Y. M. Jung, Interionic Interactions of Binary Gels Consisting of Pyrrolidinium-Based Zwitterionic Compounds and Lithium Salts, *J. Phys. Chem. B*, 2011, **115**, 1743–1750.

16 A. C. Cole, J. L. Jensen, I. Ntai, K. L. T. Tran, K. J. Weaver, D. C. Forbes and J. H. Davis, Novel Brønsted Acidic Ionic Liquids and Their Use as Dual Solvent−Catalysts, *J. Am. Chem. Soc.*, 2002, **124**, 5962–5963.

17 F. Makhlooghiazad, L. A. O'Dell, L. Porcarelli, C. Forsyth, N. Quazi, M. Asadi, O. Hutt, D. Mecerreyes, M. Forsyth and J. M. Pringle, Zwitterionic materials with disorder and plasticity and their application as non-volatile solid or liquid electrolytes, *Nat. Mater.*, 2022, **21**, 228–236.

18 Q. Shao and S. Jiang, Molecular Understanding and Design of Zwitterionic Materials, *Adv. Mater.*, 2015, **27**, 15–26.

19 M. Yoshizawa-Fujita, T. Tamura, Y. Takeoka and M. Rikukawa, Low-melting zwitterion: effect of oxyethylene units on thermal properties and conductivity, *Chem. Commun.*, 2011, **47**, 2345–2347.

20 Z. Jia, W. Yuan, C. Sheng, H. Zhao, H. Hu and G. L. Baker, Optimizing the electrochemical performance of imidazolium-based polymeric ionic liquids by varying tethering groups, *J. Polym. Sci., Part A: Polym. Chem.*, 2015, **53**, 1339–1350.

21 J. Shen, S. Feng, Y. Ling, C.-C. Chang, C. Huang, X. Wu, S. Chen, J. Liu, Y. Wu and W. Huang, Responsive Zwitterionic Polymers with Humidity and Voltage Dual-Switching for Multilevel Date Encryption and Anticounterfeiting, *Chem. Mater.*, 2021, **33**, 1477–1488.

22 J. Kaur, H. Kaur and L. G. Kaake, N and P-type zwitterion gated organic field effect transistors, *RSC Appl. Polym.*, 2024, **2**, 926–935.

23 H. Lin, Y. Xu, W. Guan, S. Zhao, X. Li, C. Zhang, C. Blecker and J. Liu, The importance of supercooled stability for food during supercooling preservation: a review of mechanisms, influencing factors, and control methods, *Crit. Rev. Food Sci. Nutr.*, 2024, **64**, 12207–12221.

24 D. Rooney, J. Jacquemin and R. Gardas, in *Ionic Liquids*, ed. B. Kirchner, Springer Berlin Heidelberg, Berlin, Heidelberg, 2009, vol. 290, pp. 185–212.

25 M. Y. Ivanov, N. V. Surovtsev and M. V. Fedin, Ionic liquid glasses: properties and applications, *Russ. Chem. Rev.*, 2022, **91**, RCR5031.

26 Q. Wang, L. Kang, X. Xu, M. Zhang, A. Chao, J. Chen, Z. Han, H. Yu, R. Li, Y. Zhao, D. Zhang and N. Jiang, Multiscale Crystalline Structure of Confined Polypeptoid Films: The Effect of Alkyl Side Chain Branching, *ACS Macro Lett.*, 2022, **11**, 1060–1066.

27 C.-U. Lee, A. Li, K. Ghale and D. Zhang, Crystallization and Melting Behaviors of Cyclic and Linear Polypeptoids with Alkyl Side Chains, *Macromolecules*, 2013, **46**, 8213–8223.

28 T. Erdmenger, J. Vitz, F. Wiesbrock and U. S. Schubert, Influence of different branched alkyl side chains on the properties of imidazolium-based ionic liquids, *J. Mater. Chem.*, 2008, **18**, 5267.

29 L. Xue, E. Gurung, G. Tamas, Y. P. Koh, M. Shadeck, S. L. Simon, M. Maroncelli and E. L. Quitevis, Effect of Alkyl Chain Branching on Physicochemical Properties of Imidazolium-Based Ionic Liquids, *J. Chem. Eng. Data*, 2016, **61**, 1078–1091.

30 K. Binnemans, Ionic Liquid Crystals, *Chem. Rev.*, 2005, **105**, 4148–4204.

31 W. Baker and C. Smyth, The Vitrification and Crystallization of Organic Molecules and the Dielectric Behavior of i-Butyl and i-Amyl Bromides, *J. Am. Chem. Soc.*, 1939, 2063–2071.

32 S. Sanmartín, J. Ramos, J. F. Vega and J. Martínez-Salazar, Strong influence of branching on the early stage of nucleation and crystal formation of fast cooled ultralong n-alkanes as revealed by computer simulation, *Eur. Polym. J.*, 2014, **50**, 190–199.

33 J. Ge, Z. Chen, Q. Ye, L. Xie, W. Song, Y. Guo, J. Zhang, X. Tong, J. Zhang, E. Zhou, Z. Wei and Z. Ge, Modulation of Molecular Stacking via Tuning 2-Ethylhexyl Alkyl Chain Enables Improved Efficiency for All-Small-Molecule Organic Solar Cells, *ACS Appl. Mater. Interfaces*, 2023, **15**, 10803–10811.

34 T. Wang, A. Peera, J. Reffner and J. M. Torkelson, Reducing the Bulk Fragility and Suppressing the Fragility-Confinement Effect in Polystyrene with Very Low Levels of 2-Ethylhexyl Acrylate Comonomer, *Macromolecules*, 2023, **56**, 3527–3537.

35 A. Satake, M. Fujita, Y. Kurimoto and Y. Kobuke, Single supramolecular porphyrin wires bridging gold nanoparticles, *Chem. Commun.*, 2009, 1231.

36 L. You, X.-F. Ren, Y. Wang, Z.-H. Ma, Y. Gu and J.-Z. Ma, "Release and Catch" Effect of Perfluoroalkylsulfonylimide-Functionalized Imidazole/Pyridine on Brønsted Acids in Organic Systems, *ChemCatChem*, 2016, **8**, 3394–3401.

37 S. Gross, D. Camozzo, V. Di Noto, L. Armelao and E. Tondello, PMMA: A key macromolecular component for dielectric low-κ hybrid inorganic–organic polymer films, *Eur. Polym. J.*, 2007, **43**, 673–696.

38 S. A. Madbouly, Broadband Dielectric Spectroscopy for Poly(methyl methacrylate)/Poly(α-methyl styrene-*co*-acrylonitrile) Blend, *Polym. J.*, 2002, **34**, 515–522.

39 K. H. Lee, S. Zhang, T. P. Lodge and C. D. Frisbie, Electrical Impedance of Spin-Coatable Ion Gel Films, *J. Phys. Chem. B*, 2011, **115**, 3315–3321.

40 H. Yan, F. Inam, G. Viola, H. Ning, H. Zhang, Q. Jiang, T. Zeng, Z. Gao and M. J. Reece, The Contribution of Electrical Conductivity, Dielectric Permittivity and Domain Switching in Ferroelectric Hysteresis Loops, *J. Adv. Dielectr.*, 2011, **01**, 107–118.

41 D. Bruch and Z.-G. Wang, A model for zwitterionic polymers and their capacitance applications, *J. Chem. Phys.*, 2024, **161**, 104901.

42 S. E. Feicht and A. S. Khair, A mathematical model for electrical impedance spectroscopy of zwitterionic hydrogels, *Soft Matter*, 2016, **12**, 7028–7037.

43 M. G. Ridwan, B. R. Shrestha, N. Maharjan and H. Mishra, Zwitterions Layer at but Do Not Screen Electrified Interfaces, *J. Phys. Chem. B*, 2022, **126**, 1852–1860.

44 M. H. Choi, K. W. Song, D. K. Moon and J. R. Haw, Effect of side chains on solubility and morphology of poly(benzodithiohene-*alt*-alkylbithiophene) in organic photovoltaics, *J. Ind. Eng. Chem.*, 2015, **29**, 120–128.

45 N. Tanio and Y. Koike, What Is the Most Transparent Polymer?, *Polym. J.*, 2000, **32**, 43–50.